Treatment of antibiotic cephalexin by heterogeneous electrochemical Fenton-based processes using chalcopyrite as sustainable catalyst

Constanza Droguett[1], Ricardo Salazar[2], Enric Brillas[3], Ignasi Sirés[3], Carlos Carlesi[4], José F. Marco[5], Abdoulaye Thiam[1]*

[1] *Programa Institucional de Fomento a la I+D+i, Universidad Tecnológica Metropolitana, Ignacio Valdivieso 2409, P.O. Box 8940577, San Joaquín, Santiago., Chile*

[2] *Laboratorio de Electroquímica del Medio Ambiente, LEQMA, Facultad de Química y Biología, Universidad de Santiago de Chile, USACh, Casilla 40, Correo 33, Santiago, Chile*

[3] *Laboratori d'Electroquímica dels Materials i del Medi Ambient, Departament de Química Física, Facultat de Química, Universitat de Barcelona, Martí i Franquès 1-11, 08028 Barcelona, Spain*

[4] *Escuela de Ingeniería de Química, Pontificia Universidad Católica de Valparaíso, Chile*

[5] *Instituto de Química Física "Rocasolano", CSIC, Madrid, Spain*

Paper submitted to be published in Science of the Total Environment

* Corresponding author: Tel.: +56227877906

E-mail address: athiam@utem.cl (A. Thiam)

Abstract

The development of heterogeneous Fenton-based electrochemical advanced oxidation processes is important for the removal of organic pollutants at industrial level in the near future. This work reports the application of heterogeneous photoelectro-Fenton (HPEF) with UVA light as an enhanced alternative to the more widespread heterogeneous electro-Fenton (HEF) process. The treatment of the antibiotic cephalexin using chalcopyrite as a sustainable catalyst was studied using an undivided IrO_2/air-diffusion cell. XPS analysis showed the presence of Fe(III), Cu(I) and Cu(II) species on the surface. The amount of Fe^{2+} ions dissolved upon chalcopyrite exposure to continuous stirring and air bubbling was proportional to chalcopyrite content. In all cases, the occurrence of pH self-regulation to an optimum value near 3 was observed. The HEF and HPEF treatments of 100 mL of 50 mg L^{-1} cephalexin solutions with 0.050 M Na_2SO_4 have been studied with 1.0 g L^{-1} chalcopyrite at 50 mA cm^{-2}. Comparative homogeneous EF and PEF with dissolved Fe^{2+} and Cu^{2+} catalysts were also performed. The HPEF process was the most effective process, which can be mainly explained by the larger production of homogeneous and heterogeneous $^{\bullet}OH$ and the photodegradation of the complexes of iron with organics. The effect of applied current and catalyst concentration on HPEF performance was assessed. Recycling experiments showed a long-term stability of chalcopyrite. Seven initial aromatics and six cyclic by-products of cephalexin were identified, and a plausible degradation route that also includes five final carboxylic acids is proposed.

Keywords: Antibiotic; Chalcopyrite; Electro-Fenton; Emerging contaminants; Heterogeneous Fenton; Photoelectro-Fenton

1. Introduction

Taking into account the risks associated to the emission of emerging contaminants, there is a need to implement measures for their management (Deblonde et al., 2011; Teodosiu et al., 2018). These pollutants do not only cause environmental problems but also threaten the human health. The scientific community and regulatory agencies are worried about the limited effectiveness of current treatments because it leads to their transfer to drinking water and food (Chapman, 2006; Benson et al., 2017). Among these pollutants, pharmaceuticals are highly accumulated in the aquatic medium due to their large use in veterinary and human medicine (Deblonde et al., 2011; Peña-Guzmán et al., 2019). The widespread use of these compounds and their persistent and toxic effects bring the necessity of developing new advanced technologies (Sirés and Brillas, 2012; Teodosiu et al., 2018).

Efforts are being made to develop sustainable and viable methods to remove organic pollutants from the environment. At industrial scale, the removal of these compounds is addressed through biological, chemical and physical processes, which are sometimes ineffective or unsuitable since they may generate highly toxic and/or stable by-products (Feng et al., 2013). These issues have promoted the development of advanced oxidation processes (AOPs), which are widely investigated for the removal of organic pollutants (Brillas and Martínez-Huitle, 2015; Martínez-Huitle et al., 2015; Martínez-Huitle and Panizza, 2018; Zhang et al., 2019a). Applications of electrochemistry in the field of AOPs have been significant due to the easy, clean and effective way to produce hydroxyl radicals ($^{\bullet}OH$) and other oxidants (Panizza and Cerisola, 2009; Sirés et al., 2014; Vasudevan and Oturan, 2014; Moreira et al., 2017). The resulting electrochemical advanced oxidation processes (EAOPs) are known to be effective for the rapid removal of target organic pollutants (Nidheesh et al., 2018). Among them, electro-Fenton (EF) and photoelectro-Fenton (PEF) have attracted great attention because of their environmental compatibility and the in situ production of hydrogen peroxide using raw and modified carbonaceous cathodes, thereby avoiding its storage and transport (Ye et al., 2019).

The EF process has become one of the most promising approaches to treat wastewater in an effective and efficient manner (Zhou et al., 2018). In EF, the weak oxidation by electrogenerated H_2O_2 is enhanced with the addition of homogeneous catalysts such as metal cations in acidic medium, according to Fenton's reaction (1) to generate homogeneous $^{\bullet}OH$ (Galia et al., 2016; Thiam et al., 2018; Zhang et al., 2019a):

$$Fe^{2+} + H_2O_2 \rightarrow Fe^{3+} + {}^{\bullet}OH + OH^- \quad (1)$$

PEF has also received considerable attention in the last decades as a useful method that allows the efficient photodegradation of stable iron complexes formed during the EF treatment (Brillas, 2014; Aguilar et al., 2017). In this process, UVA radiation coupled with EF promotes the Fe^{2+} regeneration and the production of more $^{\bullet}OH$ by reaction (2) as well as the photodecarboxylation of Fe(III) complexes with final short-chain carboxylic acids from the general reaction (3):

$$Fe(OH)^{2+} + h\nu \rightarrow Fe^{2+} + {}^{\bullet}OH \quad (2)$$

$$Fe(OOCR)^{2+} + h\nu \rightarrow Fe^{2+} + CO_2 + R^{\bullet} \quad (3)$$

Despite being promising, the industrial application of these technologies is still limited by some drawbacks. From a technical, economic and environmental point of view, some of the most important challenges for their commercialization are the restricted acid pH range, the loss of catalyst and the poor catalyst reusability (Ganiyu et al., 2018; Ye et al., 2020a). Many efforts have been made to overcome these drawbacks, like the development of heterogeneous Fenton-based electrochemical technologies. In particular, iron oxides and sulfides have been proven materials with good perspectives as heterogeneous catalysts in EF (Ganiyu et al., 2018; Ye et al., 2020b). The performance of heterogeneous electro-Fenton (HEF) with natural minerals like pyrite and chalcopyrite as catalysts has been described (Ammar et al., 2015; Barhoumi et al., 2015, 2017; Labiadh et al., 2015), allowing the easy application of treatments within a wide pH range and the catalyst reutilization (Ganiyu et al., 2018). The results showed that HEF could become more efficient than conventional EF. The use of

magnetite, goethite, hematite, and zeolite in Fenton-based processes for the removal of persistent pollutants has also been assessed (Ganiyu et al., 2018; Rezgui et al., 2018).

Chalcopyrite ($CuFeS_2$) is an iron sulfide mineral that also contains copper ions that can enhance the degradation process by producing more $^{\bullet}OH$ from the Fenton-like reaction (4) (Barhoumi et al., 2017). The exploration of iron catalysts containing other metals has gradually become a trend in the development of heterogeneous processes. In addition, aqueous chalcopyrite oxidation in the presence of oxygen results in the production of SO_4^{2-}, Fe^{2+}, Cu^{2+} and H^+ (Barhoumi et al., 2017), promoting the dosage of catalyst and self-regulation of solution pH, also reducing reagent costs. Accordingly, chalcopyrite seems a good alternative for increasing the cost-effectiveness of heterogeneous EAOPs based on Fenton's reaction. Irradiating the solution treated under HEF with UVA light could improve the efficiency from the so-called heterogeneous PEF (HPEF). Moreover, chalcopyrite presents excellent photocatalytic properties due to its high adsorption coefficient and narrow band gap (Ltaïef et al., 2018).

$$Cu^+ + H_2O_2 \rightarrow Cu^{2+} + {}^{\bullet}OH + OH^- \quad (4)$$

In order to find an upgraded alternative to heterogeneous EF processes, in this work we propose the novel HPEF treatment using chalcopyrite as a sustainable catalyst. The properties of chalcopyrite were characterized and the electrochemical degradation of the antibiotic cephalexin by electrochemical heterogeneous Fenton-based processes was investigated. Furthermore, the influence of the main parameters affecting the HPEF treatment of the antibiotic solutions was examined. The reusability of chalcopyrite was studied in successive cycles, and main by-products were identified by high-performance liquid chromatography (HPLC) with a photodiode array (PDA) or mass spectrometer as detector.

The antibiotic cephalexin (see chemical formula in Fig. SM1) was chosen as model pollutant due to its low metabolic degradation rate and its ability to induce the proliferation of antibiotic-resistant bacteria (Roth et al., 2019; Meng et al., 2020). It has been found in wastewater treatment plants and

waterways around the world (Baquero et al., 2008; Ledezma Estrada et al., 2012). Due to possible negative effects on the environment (Liu et al., 2011), several approaches have been tested for the removal of cephalexin and its by-products from aqueous medium, including biological treatment (Wang et al., 2019), ozonation (Xu et al., 2019), photocatalysis (Li et al., 2018; He et al., 2019), Fenton (Ledezma Estrada et al., 2012), photo-Fenton (Bansal et al., 2018) and homogeneous Fenton-based electrochemical processes (Ledezma Estrada et al., 2012; Antonin et al., 2019; Zhang et al., 2019b).

2. Materials and methods

2.1. Chemicals

All chemicals used in this work were of analytical grade and used without further purification. Cephalexin (98% purity), used as the target pollutant, was purchased from Sigma-Aldrich. In the homogeneous Fenton-based processes, the pH of the solution was regulated using analytical grade sulfuric acid and sodium hydroxide from Merck and Sigma-Aldrich, respectively. Iron(II) sulfate heptahydrate and copper(II) sulfate pentahydrate used as homogeneous catalysts were supplied by Merck and Labochemie, respectively. 1,10-Phenanthroline and Ti(IV) used to quantify dissolved iron and electrogenerated hydrogen peroxide were purchased from AK scientific and Sigma-Aldrich, respectively. The solutions were prepared with ultrapure water obtained from a Purelab Option-Q system with resistivity > 18.2 MΩ cm.

2.2. Characterization of chalcopyrite

Chalcopyrite, used as heterogeneous catalyst, was extracted from a mine located in Copiapó (Chile). It was milled and sieved (< 80 μm). Before use, the resulting powder was ultrasonicated in 95% ethanol, then successively cleaned with 1 M HNO_3, water and ethanol and finally dried at 30 °C. Its composition was determined by elemental analysis and the results obtained are summarized in Table 1. The Fe^{2+} leached from chalcopyrite was analyzed via the 1,10-phenantroline method using

a UV/Vis spectrometer (Prove 300 from Merck), at λ = 510 nm. Total released iron was evaluated by adding ascorbic acid. In each experiment, compressed air was bubbled into the solution at 0.6 mL min^{-1} using a diffusor. In the study of catalyst reusability, the chalcopyrite powder was cleaned with water, then ethanol and finally dried at 30 °C before reuse.

The X-ray photoelectron spectroscopy (XPS) has been the primary technique used to provide a detailed characterization of chalcopyrite. XPS was carried out with a PHOIBOS 150 System using a Mg-Kα monochromatized X-ray source (100 W) placed perpendicularly to the analyzer axis. A circular area of 0.8 mm diameter was analyzed. A low energy electron gun (less than 10 eV) was used. The general spectra in the 0-1000 eV range were recorded using a step energy of 100 eV, whereas the high resolution scans corresponding to the spectra regions of the different elements were recorded using a step energy of 20 eV. All measurements were made under ultra-high vacuum at pressures under 1×10^{-9} mbar. All binding energies were calibrated using contaminant carbon (C1s = 284.6 eV). The crystalline structure of chalcopyrite was determined by X-ray diffraction using a Bruker D8 ADVANCE diffractometer, with Cu K_α radiation (λ = 1.5418 Å) and 2θ scan from 20° to 70° (at 1^o min^{-1}). The morphology and size distribution of the mineral was examined by SEM-EDS employing a JEOL JSM-7100 F field emission scanning electron microscope at 15 kV equipped with an INCA analyzer.

2.3. Electrochemical systems

The oxidation power of HEF and HPEF using chalcopyrite as heterogeneous catalyst was evaluated using a one-compartment electrochemical cell. Solutions of 100 mL of 50 mg L^{-1} cephalexin were treated under vigorous stirring with a magnetic bar at 700 rpm. For the degradation of the antibiotic, air was bubbled through the solution at 0.6 L min^{-1} for 20 min to ensure the maximum release of ferrous iron. H_2O_2 was electrogenerated using an air-diffusion cathode purchased from E-TEK, placed in a polypropylene holder saturated with air pumped at 1 L min^{-1}. The anode was a DSA®-O_2 plate (IrO_2-based anode) from NMT Electrodes. The area of both electrodes was 2.5 cm^2

and the distance between the anode and cathode was kept at 1 cm. In the HPEF and PEF assays, the solution was irradiated with UVA light using a 6 W Philips florescent, yielding an irradiance of 5 W m^{-2}.

2.4. Instruments and procedures

Galvanostatic electrolyses were performed with an MCP (model M10-QD305) potentiostat-galvanostat. The samples were microfiltered with 0.45 μm PTFE filters from Whatman. The H_2O_2 electrogenerated was determined from the absorbance of its yellow complex formed with Ti(IV), with a maximum absorbance at 408 nm. The released copper was determined by elemental analysis. The mineralization of cephalexin solutions was assessed from their total organic carbon (TOC) decay, measured with an Elementar Vario TOC Select analyzer.

The abatement of cephalexin concentration during the electrolyses was followed by reversed-phase HPLC using a JASCO LC coupled with an MD-4015 PDA detector selected at λ = 261 nm. A GL Sciences 5020-01771 Inertsil ODS-3 (3μm, 4.6 mm × 15 mm) column was used at 30 °C. To stop the degradation processes, the aliquots were always diluted with methanol and 20 μL were injected into the chromatograph under circulation of a 75:25 (v/v) water (10 mM KH_2PO_4, pH 4.4)/methanol mixture at 1.0 mL min^{-1}.

The same chromatograph was used to quantify the short-chain carboxylic acids generated during the degradation. In this case, a SUPELCOGEL C-610H Amino (9 μm, 30 cm × 7.8 mm) column was used at 35 °C. The aliquots were injected under circulation of a 4 mM H_2SO_4 at 0.6 mL min^{-1}. The PDA detector was set at λ = 210 nm.

The aromatic by-products were detected by liquid chromatography electrospray ionization mass spectrometry (LC-ESI–MS) employing a Thermo Scientific LTQ XL linear ion trap connected to a Thermo Scientific UHPLC system equipped with a quaternary pump (UltiMate 3000 High-Speed LC System). The ESI source was set to positive and negative ion detection modes. Full scan MS data were collected for an *m/z* range of 100–2000.

3. Results and discussion

3.1. Characterization of chalcopyrite powder

The presence of chalcopyrite in the natural powder was first confirmed by XRD analysis. Fig. 1 shows a good agreement between the XRD pattern obtained and that from the diffraction data files of the Joint Committee on Powder Diffraction Standards (JCPDS, JADE 9, Materials Data Inc.). The main diffraction peaks at 29.4°, 33.9°, 49.0° and 57.8° can be attributed to the (112), (200), (204) and (312) planes, respectively, of the face-centered cubic structure of chalcopyrite. The diffractogram also shows other peaks with low intensity, which can be ascribed to the presence of impurities of other oxides or sulfides.

The surface characteristics of chalcopyrite were analyzed by XPS to determine the oxidation state of the key elements. In agreement with the elemental analysis shown in Table 1, the XPS spectra of chalcopyrite confirmed the presence of Fe, Cu and S as major elements. Iron and copper are the main metal components of chalcopyrite, which can be used to produce hydroxide radicals, and their respective high-resolution spectra are depicted in Fig. 2. The XPS peaks of Fe 2p, Cu 2p and S 2p always appeared as doublets due to the spin-orbit splitting, with the $2p_{3/2}$ peak being two times higher than the $2p_{1/2}$ one. The high-resolution spectrum showed peaks ranging across reported binding energies of 710-725 eV, corresponding to Fe $2p_{1/2}$ and Fe $2p_{2/3}$. The Fe 2p spectrum was fitted using a 2:1 peak area ratio for Fe $2p_{3/2}$ and Fe $2p_{1/2}$ and 13.1 eV splitting. The peaks fitted to the spectrum using a summed Gaussian-Lorentzian (GL) function. The Fe 2p spectrum contained contributions from Fe(III)-S and Fe(III)-O bonds peaked at 708.4 and 714.3 eV, respectively (Mikhlin et al., 2016), respectively. The others were secondary peaks due to splitting or “shake up” satellites, but corresponded to the Fe(III) species. Fig. 2b depicts the high-resolution spectrum of Cu 2p. Copper existed in the valence +1 (Cu^{+}), which corresponded to the two strongest peaks centred at bonding energy of 932.3 and 952.3 eV. Extensive oxidation of chalcopyrite surfaces often yield the formation of copper hydroxide, with copper in the form of Cu^{2+}. The peaks located to 934.3 and 954.3 eV

correspond to Cu $2p_{3/2}$ and Cu $2p_{1/2}$ of Cu^{2+}, respectively. Also, the presence of Cu^{2+} usually results in the appearance of a satellite peak whose binding energy is around 942 eV (Ghahremaninezhad et al., 2013). In the case of the Cu 2p spectrum presented, this signal is observed, confirming the divalent state of copper (Cu^{2+}). The XPS analysis clearly showed the presence of Cu(I), Fe(III) and S(II) (data not shown), indicating that chalcopyrite is present in the powder in the form of $Cu^{+}Fe^{+3}S^{-2}$, i.e., $CuFeS_2$.

The morphology and size distribution of the mineral particles was examined by SEM. Fig. SM2a-d shows the SEM images of the chalcopyrite powder before use. The microparticles had different shapes and sizes, with the main length ranging from 10 to 90 μm (Fig. SM2b). The SEM images highlight the presence of two main phases, related to grey and dark-grey color regions. This difference suggests that chalcopyrite was accompanied by a hosting mineral, which could justify the additional peaks observed in the XRD patterns. The TEM analysis of Fig. 3a shows a typical microparticle with irregular shape. In addition, the distribution of iron and copper throughout the particle surface was determined by EDS mapping. From Fig. 3b and c, the homogenous distribution of both metals is evident, with around 27 wt.% and 26 wt.%, respectively, as theoretically expected. The EDS analysis in Fig. 3d confirms the presence of S, Fe and Cu as main components of chalcopyrite, as determined in the elemental analysis.

Prior to monitor the treatment of cephalexin by Fenton-based EAOPs, the effect of mineral content on Fe^{2+}/Fe^{3+} leaching, as well as the time course of solution pH, were studied in order to determine the optimum conditions to carry out the degradation trials. The influence of chalcopyrite content on the concentration of dissolved Fe^{2+} was evaluated in a range from 1 to 10 g L^{-1} in 100 mL of ultrapure water. The suspensions were continuously saturated with O_2 by bubbling compressed air at 0.6 L min^{-1}. It can be observed in Fig. 4 that the Fe^{2+} concentration, measured at 30 min, increased at a greater chalcopyrite loading, which is related to the larger metal ion release according to reactions (5)-(7). The time course of Fe^{2+} and total iron concentrations is reported in Fig. SM3a. In all cases,

the concentration of both species gradually grew for 20 min, whereupon steady concentrations were reached without further significant changes. This behavior can be explained by the equilibrium reached by the three mentioned reactions at that time. The corresponding evolution of the solution pH is presented in Fig. SM3b. Similar profiles for pH decay can be observed regardless of the initial chalcopyrite load. The solution pH initially decreased from about 5 to about 3, and a steady state was reached at about 20 min, confirming that the equilibrium of reactions (5)-(7) was reached. The results demonstrate that chalcopyrite can be potentially used as a sustainable heterogeneous catalyst, since it allows the occurrence of dissolved Fe^{2+} (and Cu^{2+}) ions, as well as the pH self-regulation to a value close to 3. Note that, in fact, this is the optimum pH to carry out the homogeneous Fenton's reaction (Sirés and Brillas, 2012).

$$CuFeS_2 + 4O_2 \rightarrow Cu^{2+} + Fe^{2+} + 2SO_4^{2-} \quad (5)$$

$$CuFeS_2 + 4H^+ + O_2 \rightarrow Cu^{2+} + Fe^{2+} + 2S^0 + 2H_2O \quad (6)$$

$$CuFeS_2 + 16Fe^{3+} + 8H_2O \rightarrow Cu^{2+} + 17Fe^{2+} + 2SO_4^{2-} + 16H^+ \quad (7)$$

3.2. Electrogeneration of H_2O_2 with and without chalcopyrite

The efficiency of Fenton-based processes depends on the capacity of the cathode used to generate H_2O_2 on site. Therefore, the effect of current density on the H_2O_2 production when using an air-diffusion cathode, with or without chalcopyrite, was assessed. Fig. SM4 exhibits the evolution of H_2O_2 over the electrolysis. A larger H_2O_2 accumulation can be observed when the current density was increased, owing to the quicker reduction of oxygen at the cathode surface as a result of the faster electron supply. The H_2O_2 concentration gradually attained a quasi-steady value as the electrolysis was prolonged. This behavior can be related to the simultaneous destruction of a similar quantity of H_2O_2 at the anode of the undivided cell (Thiam and Salazar, 2019). In order to evaluate the efficiency of chalcopyrite as a sustainable catalyst for Fenton-based EAOPs, the accumulation of H_2O_2 in the presence of the mineral powder was determined. Fig. SM4 shows that the concentration of H_2O_2

dropped from 44.0 to 4.5 mM (10 times) in the presence of 1 g L^{-1} after 240 min of electrolysis at 50 mA cm^{-2}. This result can be explained by the H_2O_2 consumption, via reaction with released iron and copper ions in the bulk as well as on the chalcopyrite surface, producing $^{\bullet}OH$ from homogeneous and heterogeneous Fenton's reaction, respectively.

3.3. Treatment of cephalexin solutions by Fenton-based EAOPs

Fig. 5 compares the degradation of 100 mL of 50 mg L^{-1} of cephalexin solutions with 0.050 M Na_2SO_4 and 1 g L^{-1} chalcopyrite by various methods. Fig. 5a presents the profile of cephalexin concentration during the HEF and HPEF treatments, where a fast and complete removal was attained in both cases. The quick abatement of the antibiotic can be related to the production of a large amount of $^{\bullet}OH$ via two mechanisms: homogeneous catalysis with dissolved iron and copper ions and heterogeneous catalysis on the chalcopyrite surface. Additionally, copper cations can promote the Fe^{2+} regeneration (Salazar et al., 2012), which maintains the Fe^{3+}/Fe^{2+} catalytic cycle for Fenton process. Simultaneously, cephalexin can be oxidized by $IrO_2(^{\bullet}OH)$ formed at the anode surface (Brillas and Martínez-Huitle, 2015). The HPEF process led to a superior antibiotic removal because at 15 min the complete concentration decay was observed, whereas 94.0 % was achieved by HEF (Table 2). The latter process needed 30 min to reach 100% removal. The difference in both processes can be mainly related to the additional production of $^{\bullet}OH$ from the photolysis of the highly photoactive Fe(III) species via reaction (2). The potential contribution of other mechanism is discussed below.

The kinetics associated to those cephalexin decays during HEF and HPEF were analyzed considering different reaction orders, finding good linear correlations for a pseudo-first-order reaction. The superiority of HPEF was confirmed by the rate constants obtained through the kinetic analysis shown in the inset of Fig. 5a. The apparent rate constants (k_1) were 3.12×10^{-3} and 4.85×10^{-3} s^{-1} in HEF and HPEF, respectively (see Table 2). The removal of cephalexin by HPEF was then 1.5 times greater, confirming the very positive role of UVA irradiation.

Since the removals commented above could potentially have different contributions, an additional set of trials was carried out to gain further insight. The processes under study were: (i) adsorption on chalcopyrite powder, (ii) photolysis (irradiation with only UVA light), (iii) chalcopyrite/UVA photocatalysis (irradiation of the suspension containing chalcopyrite). Fig. 5b depicts the percentage of cephalexin removal after 15 min of each treatment, including the HPEF result from Fig. 5a. Pure adsorption on the catalyst surface led to the slowest disappearance, being as low as 2% at that time. An analogous slow removal percentage was achieved during pure photolysis with UVA light, suggesting the low photolytic activity of cephalexin. In contrast, Fig. 5b discloses a faster antibiotic abatement using the chalcopyrite/UVA system, with a degradation of 38.6%. From the two latter results, the role of chalcopyrite as photocatalyst can be inferred. This supports the results presented in Fig. 5a and is in agreement with results reported by Ltaief et al. (2018), who found a substantial light absorption for chalcopyrite ranging from the near UV to the visible region and detailed a much quicker degradation of tyrosol by photo-Fenton as compared to Fenton using chalcopyrite as heterogeneous catalyst. Based on this, the overall disappearance of cephalexin by HPEF in 15 min (see Fig. 5b) can be related to its photocatalysis stimulated by chalcopyrite along with the participation of photo-Fenton reaction (2).

The influence of key experimental variables on the HPEF performance was analyzed in order to optimize the process. Current density and catalyst concentration are the most important variables governing the efficiency of the process. The effect of current density for the treatment of 50 mg L^{-1} cepholaxin with 0.050 M Na_2SO_4 and 1 g L^{-1} chalcopyrite using an IrO_2/air diffusion cell is presented in Fig. SM5. The antibiotic abatement was enhanced with increasing the current density from 25 to 100 mA cm^{-2}. A similar trend can be observed for the corresponding k_1-values listed in Table 2. This positive trend can be simply related to the gradual rise in the quantity of electrogenerated H_2O_2 at any given time (see Fig. SM4), yielding more $^{\bullet}OH$ in the bulk from Fenton's reaction. The final percentages of cephalexin removal were very similar at 50 and 100 mA cm^{-2}. This loss of efficiency

when increasing the current density can be explained by the larger waste of the electric energy supplied due to the acceleration of side reactions that destroy the $IrO_2(^{\bullet}OH)$ and $^{\bullet}OH$. These reactions can be the anodic oxidation of $IrO_2(^{\bullet}OH)$ to evolve O_2 and the reaction of $^{\bullet}OH$ with H_2O_2 to form the weak hydroperoxyl radical $HO_2^{\bullet}$ (Lanzalaco et al., 2018; Thiam and Salazar, 2019). From these results, 50 mA cm^{-2} was chosen as optimum value to carry out the rest of the experiments.

Chalcopyrite content is considered crucial in the HPEF process, since the presence of this catalyst offers a predominant route to destroy the antibiotic under the main action of $^{\bullet}OH$. To understand the effect of this parameter on cephalexin removal, a series of experiments at different catalyst contents (0.5, 1.0, 2.0 and 3.0 g L^{-1}) was carried out. As can be seen in Fig. 6, the increase from 0.5 to 1.0 g L^{-1} enhanced the degradation rate, yielding total drug removal within 30 and 15 min, respectively. This tendency can be attributed to the greater production of oxidant $^{\bullet}OH$ from Fenton's reaction (1) and Fenton-like reaction (4) due to the increase of Fe^{2+} and Cu^{+} concentration when the chalcopyrite load was increased (see Fig. SM3). Conversely, beyond 1.0 g L^{-1} chalcopyrite, the degradation rate decreased and total removal was reached after 30 min of electrolysis at 2.0 and 3.0 g L^{-1}. This decrease can be attributed to the reaction of $^{\bullet}OH$ with excess of dissolved Fe^{2+} by reaction (8) (a similar reaction with Cu^{+} cannot be discarded). This is reflected in the maximum k_1-value of 4.85×10^{-3} s^{-1} found at 1.0 g L^{-1}, also attaining the lowest EC_{TOC} value (see Table 2), thus becoming the optimal value for the HPEF process.

$$Fe^{2+} + {}^{\bullet}OH \rightarrow Fe^{3+} + OH^{-} \quad (8)$$

Once established the optimum operating parameters for an effective heterogeneous process, a comparison with homogeneous electro-Fenton (EF) and photoelectro-Fenton (PEF) was made. From the results obtained in Section 3.1, these homogeneous processes were performed by adding 0.05 mM Fe^{2+} + 0.05 mM Cu^{2+} and adjusting the pH to 3.0, while the heterogeneous processes used 1 g L^{-1} chalcopyrite without previous adjustment of the pH. In Fig. 7a, the concentration abatement of 50 mg L^{-1} cephalexin with 0.050 M Na_2SO_4 using the different catalyst in an IrO_2/air-diffusion cell at

317 50 mA cm^{-2} is depicted. A faster antibiotic degradation was achieved using heterogeneous catalysts.
318 Table 2 shows an increasing cephalexin removal of 77.6%, 82.4%, 94.0% and 100% for EF, PEF,
319 HEF and HPEF, respectively, after 15 min of treatment. Thus, significantly lower k_1-values were
320 obtained for the homogeneous processes from the good linear profiles depicted in the inset of Fig. 7a
321 (see Table 2). The faster cephalexin degradation using HEF as compared to homogeneous EF and
322 PEF suggests a greater generation of $^{\bullet}OH$ by heterogeneous reaction of H_2O_2 with surface Fe^{2+} and
323 Cu^{+} ions, although the positive effect of the controlled metal ion dosage to react with H_2O_2 in the
324 bulk cannot be discarded either. In the case of HPEF, such metal ion release could be higher due to
325 promotion by UV illumination (Zhou et al., 2015), which would add to the photocatalysis process on
326 the surface and the photo-Fenton process in the bulk.
327 A typical problem in the treatment of organic pollutants is the generation of organic by-products
328 that can be more toxic and persistent than the target molecule. The TOC decay for the above
329 heterogeneous and homogeneous Fenton-based EAOPs is illustrated in Fig. 7b. The HEF process was
330 the less powerful, presenting only 43.5% TOC decay after 300 min of electrolysis, probably due to
331 the generation of recalcitrant intermediates such as short-chain carboxylic acids. In contrast, in the
332 photoassisted Fenton-based process, a much quicker mineralization rate can be observed, achieving
333 80.0 and 92.0% TOC removal in PEF and HPEF, respectively. The superiority of the two latter
334 processes is due to the action of the radiation used in the degradation process. Cephalexin and its by-
335 products can plausibly lead to the formation of short-chain carboxylic acids (see below). These acids
336 easily form complexes with Fe(III), being refractory to $^{\bullet}OH$ but effectively photodegraded by UV
337 photons according to reaction (3). The HPEF process with chalcopyrite showed a higher
338 mineralization as compared to homogeneous PEF, thus confirming that the heterogeneous catalyst is
339 beneficial in photoassisted Fenton-based processes.

The analysis of the final solution in HPEF revealed the total conversion of S of cephalexin into SO_4^{2-} ion and that of 65% of the initial N into NO_3^- ion. From this, the total mineralization of the drug can be written as observed in reaction (9), with a number of electrons n = 70.

$$C_{16}H_{17}N_3O_4S + 32H_2O \rightarrow 16CO_2 + 3NH_4^+ + SO_4^{2-} + 69H^+ + 70e^- \quad (9)$$

The mineralization current efficiency (MCE) was then estimated through Eq. (10) (Steter et al., 2018).

$$\text{MCE (\%)} = \frac{(\Delta \text{TOC})_{\text{exp}}\, n\, F\, V_s}{4.32 \times 10^7\, m\, I\, t} \times 100 \quad (10)$$

where $\Delta(\text{TOC})_{\text{exp}}$ is the experimental TOC decay (in mg L^{-1}), F is the Faraday's constant (96487 C mol^{-1}), V_s is the solution volume (in L), 4.32×10^7 is a conversion factor for unit homogenization (3600 s h^{-1} × 12000 mg carbon mol^{-1}), m is the number of carbon atoms of cephalexin, I is the applied current (in A) and t is the electrolysis time (in s).

Fig. 7c illustrates the evolution of MCE during the cephalexin treatments of Fig. 7b. As expected, the highest current efficiency was obtained in HPEF, which drastically dropped down from 15.5% at 30 min to 4.0% at 300 min. This behavior confirms the high catalytic ability of chalcopyrite. In all cases, the MCE values decreased at longer electrolysis time, which can be related to the accumulation of compounds with a higher refractoriness to $^{\bullet}OH$ along with a promotion of the wasting reactions that destroy the reactive radicals in the absence of enough organic matter.

From the TOC abatement, the energy consumption per unit TOC mass (EC_{TOC}) was calculated from Eq. (11) (Steter et al., 2018):

$$EC_{TOC}\ (\text{kWh (g TOC)}^{-1}) = \frac{E_{\text{cell}}\, I\, t}{V_s\, \triangle(\text{TOC})_{\text{exp}}} \quad (11)$$

where E_{cell} is the average cell voltage (in V) and the rest of parameters have been defined from Eq. (10) although time t is now expressed in hours.

362 According to the trends obtained for the TOC removals and MCE, the EC_{TOC} in HPEF was the
363 lowest. Final EC_{TOC} values of 8.67 and 4.69 kWh $(g\ TOC)^{-1}$ were found in HEF and PEF,
364 respectively, higher than 4.07 kWh $(g\ TOC)^{-1}$ determined in HPEF.

365 The above results confirm the benefits of using chalcopyrite as a catalyst in the HPEF process.
366 Additionally, the use of chalcopyrite can favour the catalyst reutilization, which could make these
367 processes more sustainable for continuous treatment. The reusability is an important feature of
368 heterogeneous catalysts. To evaluate this, the evolution of the percentage of cephalexin removal for
369 20 min was assessed in 4 successive cycles by means of the HPEF process. In each cycle, a fresh
370 solution of 50 mg L^{-1} cephalexin with 0.050 M Na_2SO_4 was electrolyzed at 50 mA cm^{-2}. Chalcopyrite
371 was added at 1 g L^{-1}, being recycled via filtration, cleaning with ultrapure water and ethanol, and
372 drying under an air flow. Fig. 8 shows that complete cephalexin abatement was reached after 15 min
373 in each of the 4 successive cycles, confirming its stability during the treatment of persistent emerging
374 pollutants.

375 *3.4. By-products and reaction sequence for cephalexin removal*

376 For a better understanding of cephalexin mineralization by means of heterogeneous Fenton-
377 based EAOPS, ion-exclusion HPLC was conducted to identify the final short-chain carboxylic acids.
378 This kind of by-product has been found during the mineralization of aromatic pollutants (Oturan et
379 al., 2008; Salazar et al., 2012). To do this, chromatograms resulting from the injection of samples
380 from solutions treated under the conditions of Fig. 5 were recorded, allowing identifying a mixture
381 of carboxylic acids including maleic, fumaric, oxalic, formic and oxamic acids. According to their
382 structures, maleic and fumaric acids were formed from the cleavage of the linear and cyclic parts of
383 cephalexin. Both acids were formed and degraded at a similar rate and therefore, they were always
384 detected in residual amounts. Both acids can justify the formation of oxalic and formic acids, which
385 can also be produced directly from the breakage of cephalexin. Oxamic acid could be formed from
386 the oxidation of *N*-containing by-products. The three latter acids are ultimate by-products that are

converted into CO_2. In Fenton-based processes, it is well known that oxalic and oxamic acids are the most persistent acids and their removal is key for the efficiency of the processes (Thiam and Salazar, 2019; Thiam et al., 2018). The evolution of both acids during the HEF and HPEF treatments of cephalexin is depicted in Fig. 9. The concentration of oxalic acid increased progressively in HEF up to attain a maximal of 20 mg L^{-1} at 240 min, which remained constant over time. This accumulation is due to the formation of Fe(III)-oxalate complexes that cannot be removed by generated $^{\bullet}OH$. Irradiating the system in the HPEF process allowed the photolysis of the Fe(III) complex from reaction (3), causing the acid disappearance at 240 min. A similar behavior can be observed with oxamic acid, although its accumulation was lower than that of oxalic acid in HEF, and it was only partially photodegraded in HPEF. The positive photolytic action of UVA light is in agreement with the superior mineralization of HPEF over HEF.

The primary by-products formed during the HEF and HPEF treatments of 50 mg L^{-1} cephalexin with 0.050 M Na_2SO_4 and 1.0 g L^{-1} chalcopyrite were identified by LC-ESI-MS and a reaction route is proposed in Fig. 10, where $^{\bullet}OH$ is the main oxidant. Taking into account their structure, the intermediates were classified in 5 groups (A, B, C, D and E). The degradation route was initiated by the cleavage of the β-lactam ring of cephalexin, leading to the formation of 2-amino-*N*-[1-(5-methyl-3,6-dihydro-2H-[1,3]thiazin-2-yl)-2-oxo-ethyl]-2-phenyl-acetamide (**A1**). **A1** underwent further oxidation, resulting in the opening of the cephalosporin ring and hydroxylation, finally yielding 2-amino-N-[1-hydroxy-2-(2-hydroxy-ethylamino)-2-mercapto-ethyl]-2-phenyl-acetamide (**A2**). Alternatively, the cleavage of the $C_{aliphatic}$-N of the nitrogen linked to the cephalosporin ring of cephalexin, alongside demethylation and hydroxylation, gave 7-amino-3-hydroxy-8-oxo-5-thia-1-aza-bicyclo[4.2.0]oct-2-ene-2-carboxylic acid (**B1**). Additionally, the cleavage of $N_{aliphatic}$-$C_{cephalosporin}$ of cephalexin produced 3-methyl-8-oxo-5-thia-1-aza-bicyclo[4.2.0]oct-2-ene-2-carboxylic acid (**B2**). Further deamination of **B1** led to 3,8-dihydroxy-5-thia-1-aza-bicyclo[4.2.0]oct-2-ene-2-carboxylic acid (**B3**), which can also be formed from **B2**. Compounds of the group **C** were

generated from those of group **A**, initiated from the cleavage of the C-CS bond of **A2** to form 2-amino-N-hydroxymethyl-2-phenyl-acetamide **(C1)**, which further gaves 2-amino-2-phenyl-acetamide **(C2)** from the cleavage of the N-CHOH bond. Subsequently, the hydroxylation of the aromatic ring or deamination of **C2** yielded 2-amino-2-(3-hydroxyphenyl)-acetamide **(C3)** or amino-phenyl-acetaldehyde **(C4),** respectively. Amino-(3-hydroxy-phenyl)-acetaldehyde **(C5)** was originated from the deamination or hydroxylation of **C3** or **C4,** respectively. On the other hand, 2-aminomethyl-3,5-dihydroxy-3,6-dihydro-2H-[1,3]thiazine-4-carboxylic acid **(D1)** came from the cleavage of the N-CO bond of **A1** and the opening of the β-lactam ring of **B1**. The cleavage of the $C_{aliphatic}$-C_{ring} bond of **D1** led to 3,5-dihydroxy-3,6-dihydro-2H-[1,3]thiazine-4-carboxylic acid **(D2)**. Finally, **B1** and **B2** gave C-(2-methylbut-2-enylsulfanyl)-methylamine (**E**) from the cleavage of the cephalosporin ring. The subsequent degradation of these intermediates yielded the mixture of short-chain carboxylic acids described above.

4. Conclusions

This study provides a novel strategy using natural minerals with simultaneous UVA irradiation to improve the efficiency of wastewater treatment technologies as an approach for industrial scale application. Chalcopyrite, a non-toxic natural mineral, has been successfully used for the degradation and mineralization of cephalexin by Fenton-based processes. Leaching of iron and copper ions is one of the mechanisms for the formation of $^{\bullet}OH$ by reaction with electrogenerated H_2O_2. Under UVA illumination, photocatalysis is another important pathway for the antibiotic removal. The concentration of released Fe^{2+} was found to be proportional to the chalcopyrite load and a spontaneous regulation of solution pH to an optimum value near 3 for the Fenton's reaction was reached. From the point of view of cephalexin removal and mineralization, HPEF outperformed HEF and homogeneous Fenton-based processes. A chalcopyrite load of 1.0 g L^{-1} and a current density of 50 mA cm^{-2} were found as the optimum operation parameters in HPEF, given the efficient cephalexin

removal and low energy consumption. For all experimental conditions tested, the antibiotic abatement obeyed a pseudo-first-order reaction. The long-term stability of the chalcopyrite has been demonstrated by reutilizing the mineral in 4 successive cycles. A plausible reaction sequence for cephalexin degradation was proposed based on the 7 aromatic and 6 cyclic intermediates identified by LC-ESI-MS. Maleic, fumaric, oxalic, formic and oxamic acids were detected by ion-exclusion HPLC as final carboxylic acids.

Acknowledgments

Financial support from FONDECYT project 11180772 (CONICYT, Chile) as well as from project CTQ2016-8616-R (AEI/FEDER, EU) is acknowledged. A. Thiam is grateful to the 'Becas Iberoamérica. Santander Universidades' program.

Conflict of Interest: The authors declare that they have no conflict of interest.

References

Aguilar, Z.G., Brillas, E., Salazar, M., Nava, J.L., Sirés, I., 2017. Evidence of Fenton-like reaction with active chlorine during the electrocatalytic oxidation of Acid Yellow 36 azo dye with Ir-Sn-Sb oxide anode in the presence of iron ion. Appl. Catal. B: Environ. 206, 44–52. http://dx.doi.org/10.1016/j.apcatb.2017.01.006

Ammar, S., Oturan, M.A., Labiadh, L., Guersalli, A., Abdelhedi, R., Oturan, N., Brillas, E., 2015. Degradation of tyrosol by a novel electro-Fenton process using pyrite as heterogeneous source of iron catalyst. Water Res. 74, 77–87. https://doi.org/10.1016/j.watres.2015.02.006

Antonin, V.S., Aquino, J.M., Silva, B.F., Silva, A.J., Rocha-Filho, R.C., 2019. Comparative study on the degradation of cephalexin by four electrochemical advanced oxidation processes: Evolution of oxidation intermediates and antimicrobial activity. Chem. Eng. J. 372, 1104–1112.

https://doi.org/10.1016/j.cej.2019.04.185

Bansal, P., Verma, A., Mehta, C., Singla, J., Toor, A.P., 2018. Assessment of integrated binary process by coupling photocatalysis and photo-Fenton for the removal of cephalexin from aqueous solution. J. Mater. Sci. 53, 7326–7343. https://doi.org/10.1007/s10853-018-2094-x

Baquero, F., Martínez, J.L., Cantón, R., 2008. Antibiotics and antibiotic resistance in water environments. Curr. Opin. Biotechnol. 19, 260–265. https://doi.org/10.1016/j.copbio.2008.05.006

Barhoumi, N., Labiadh, L., Oturan, M.A., Oturan, N., Gadri, A., Ammar, S., Brillas, E., 2015. Electrochemical mineralization of the antibiotic levofloxacin by electro-Fenton-pyrite process. Chemosphere 141, 250–257. https://doi.org/10.1016/j.chemosphere.2015.08.003

Barhoumi, N., Olvera-Vargas, H., Oturan, N., Huguenot, D., Gadri, A., Ammar, S., Brillas, E., Oturan, M.A., 2017. Kinetics of oxidative degradation/mineralization pathways of the antibiotic tetracycline by the novel heterogeneous electro-Fenton process with solid catalyst chalcopyrite. Appl. Catal. B: Environ. 209, 637–647. https://doi.org/10.1016/j.apcatb.2017.03.034

Benson, R., Conerly, O.D., Sander, W., Batt, A.L., Boone, J.S., Furlong, E.T., Glassmeyer, S.T., Kolpin, D.W., Mash, H.E., Schenck, K.M., Simmons, J.E., 2017. Human health screening and public health significance of contaminants of emerging concern detected in public water supplies. Sci. Total Environ. 579, 1643–1648. https://doi.org/10.1016/j.scitotenv.2016.03.146

Brillas, E., 2014. A review on the degradation of organic pollutants in waters by UV photoelectro-Fenton and solar photoelectro-Fenton. J. Braz. Chem. Soc. 25, 393–417. https://doi.org/10.5935/0103-5053.20130257

Brillas, E., Martínez-Huitle, C.A., 2015. Decontamination of wastewaters containing synthetic organic dyes by electrochemical methods. An updated review. Appl. Catal. B: Environ. 166–167, 603–643. https://doi.org/10.1016/j.apcatb.2014.11.016

Chapman, P.M., 2006. Emerging substances - Emerging problems? Environ. Toxicol. Chem. 25,

1445–1447. https://doi.org/10.1897/06-025.1

Deblonde, T., Cossu-Leguille, C., Hartemann, P., 2011. Emerging pollutants in wastewater: A review of the literature. Int. J. Hyg. Environ. Health 214, 442–448. https://doi.org/10.1016/j.ijheh.2011.08.002

Feng, L., van Hullebusch, E.D., Rodrigo, M.A., Esposito, G., Oturan, M.A., 2013. Removal of residual anti-inflammatory and analgesic pharmaceuticals from aqueous systems by electrochemical advanced oxidation processes. A review. Chem. Eng. J. 228, 944–964. https://doi.org/10.1016/j.cej.2013.05.061

Galia, A., Lanzalaco, S., Sabatino, M.A., Dispenza, C., Scialdone, O., Sirés, I., 2016. Crosslinking of poly(vinylpyrrolidone) activated by electrogenerated hydroxyl radicals: A first step towards a simple and cheap synthetic route of nanogel vectors. Electrochem. Commun.62, 64–68. http://dx.doi.org/10.1016/j.elecom.2015.12.005

Ganiyu, S.O., Zhou, M., Martínez-Huitle, C.A., 2018. Heterogeneous electro-Fenton and photoelectro-Fenton processes: A critical review of fundamental principles and application for water/wastewater treatment. Appl. Catal. B: Environ. 235, 103–129. https://doi.org/10.1016/j.apcatb.2018.04.044

Ghahremaninezhad, A., Dixon, D.G., Asselin, E., 2013. Electrochemical and XPS analysis of chalcopyrite ($CuFeS_2$) dissolution in sulfuric acid solution. Electrochim. Acta 87, 97–112. https://doi.org/10.1016/j.electacta.2012.07.119

He, J., Zhang, Y., Guo, Y., Rhodes, G., Yeom, J., Li, H., Zhang, W., 2019. Photocatalytic degradation of cephalexin by ZnO nanowires under simulated sunlight: Kinetics, influencing factors, and mechanisms. Environ. Int. 132, 105105. https://doi.org/10.1016/j.envint.2019.105105

Labiadh, L., Oturan, M.A., Panizza, M., Hamadi, N. Ben, Ammar, S., 2015. Complete removal of AHPS synthetic dye from water using new electro-fenton oxidation catalyzed by natural pyrite as heterogeneous catalyst. J. Hazard. Mater. 297, 34–41.

https://doi.org/10.1016/j.jhazmat.2015.04.062

Lanzalaco, S., Sirés, I., Galia, A., Sabatino, M.A., Dispenza, C., Scialdone, O., 2018. Facile crosslinking of poly(vinylpyrrolidone) by electro-oxidation with IrO_2-based anode under potentiostatic conditions. J. Appl. Electrochem. 48, 1343–1352. https://doi.org/10.1007/s10800-018-1237-8

Ledezma Estrada, A., Li, Y.-Y., Wang, A., 2012. Biodegradability enhancement of wastewater containing cefalexin by means of the electro-Fenton oxidation process. J. Hazard. Mater. 227–228, 41–48. https://doi.org/10.1016/J.JHAZMAT.2012.04.079

Li, N., Tian, Y., Zhao, J., Zhang, J., Zuo, W., Kong, L., Cui, H., 2018. Z-scheme 2D/3D g-C_3N_4@ZnO with enhanced photocatalytic activity for cephalexin oxidation under solar light. Chem. Eng. J. 352, 412–422. https://doi.org/10.1016/J.CEJ.2018.07.038

Liu, H., Liu, W., Zhang, J., Zhang, C., Ren, L., Li, Y., 2011. Removal of cephalexin from aqueous solutions by original and Cu(II)/Fe(III) impregnated activated carbons developed from lotus stalks Kinetics and equilibrium studies. J. Hazard. Mater. 185, 1528–1535. https://doi.org/10.1016/j.jhazmat.2010.10.081

Ltaïef, A.H., Pastrana-Martínez, L.M., Ammar, S., Gadri, A., Faria, J.L., Silva, A.M.T., 2018. Mined pyrite and chalcopyrite as catalysts for spontaneous acidic pH adjustment in Fenton and LED photo-Fenton-like processes, J. Chem. Technol. Biotechnol. 93, 1137-1146. https://doi.org/10.1002/jctb.5472

Martínez-Huitle, C.A., Panizza, M., 2018. Electrochemical oxidation of organic pollutants for wastewater treatment. Curr. Opin. Electrochem. 11, 62-71. https://doi.org/10.1016/j.coelec.2018.07.010

Martínez-Huitle, C.A., Rodrigo, M.A., Sirés, I.; Scialdone, O., 2015. Single and coupled electrochemical processes and reactors for the abatement of organic water pollutants: a critical review

Meng, L., Wang, J., Li, X., Cui, F., 2020. Insight into effect of high-level cephalexin on fate and driver mechanism of antibiotics resistance genes in antibiotic wastewater treatment system. Ecotoxicol. Environ. Safe. 201, 110739. https://doi.org/10.1016/j.ecoenv.2020.110739

Mikhlin, Y., Romanchenko, A., Tomashevich, Y., Shurupov, V., 2016. Near-surface regions of electrochemically polarized chalcopyrite ($CuFeS_2$) as studied using XPS and XANES. Phys. Proc. 84, 390–396. http://doi: 10.1016/j.phpro.2016.11.067

Moreira, F.C., Boaventura, R.A.R., Brillas, E., Vilar, V.J.P., 2017. Electrochemical advanced oxidation processes: A review on their application to synthetic and real wastewaters. Appl. Catal. B: Environ. 202, 217–261. https://doi.org/10.1016/j.apcatb.2016.08.037

Nidheesh, P. V., Zhou, M., Oturan, M.A., 2018. An overview on the removal of synthetic dyes from water by electrochemical advanced oxidation processes. Chemosphere 197, 210–227. https://doi.org/10.1016/j.chemosphere.2017.12.195

Oturan, M.A., Guivarch, E., Oturan, N., Sirés, I., 2008. Oxidation pathways of malachite green by Fe^{3+}-catalyzed electro-Fenton process. Appl. Catal. B: Environ. 82, 244–254. https://doi.org/10.1016/j.apcatb.2008.01.016

Panizza, M., Cerisola, G. 2009. Direct and mediated anodic oxidation of organic pollutants. Chem. Rev. 109, 6541-6569. https://doi.org/10.1021/cr9001319

Peña-Guzmán, C., Ulloa-Sánchez, S., Mora, K., Helena-Bustos, R., Lopez-Barrera, E., Alvarez, J., Rodriguez-Pinzón, M., 2019. Emerging pollutants in the urban water cycle in Latin America: A review of the current literature. J. Environ. Manage. 237, 408–423. https://doi.org/10.1016/j.jenvman.2019.02.100

Rezgui, S., Amrane, A., Fourcade, F., Assadi, A., Monser, L., Adhoum, N., 2018. Electro-Fenton catalyzed with magnetic chitosan beads for the removal of Chlordimeform insecticide. Appl. Catal. B: Environ. 226, 346–359. https://doi.org/10.1016/j.apcatb.2017.12.061

Roth, N., Hofacre, C., Zitz, U., Mathis, G.F., Moder, K., Doupovec, B., Berghouse, R., Doming, K.J., 2019. Prevalence of antibiotic-resistant *E. coli* in broilers challenged with a multi-resistant *E. coli* strain and received ampicillin, an organic acid-based feed additive or a synbiotic preparation. Microbiol. Food Safe. 98. 2598-2607. http://dx.doi.org/10.3382/ps/pez004

Salazar, R., Brillas, E., Sirés, I., 2012. Finding the best Fe^{2+}/Cu^{2+} combination for the solar photoelectro-Fenton treatment of simulated wastewater containing the industrial textile dye Disperse Blue 3. Appl. Catal. B: Environ. 115–116, 107–116. https://doi.org/10.1016/j.apcatb.2011.12.026

Sirés, I., Brillas, E., 2012. Remediation of water pollution caused by pharmaceutical residues based on electrochemical separation and degradation technologies: A review. Environ. Int. 40, 212–229. https://doi.org/10.1016/j.envint.2011.07.012

Sirés, I., Brillas, E., Oturan, M.A., Rodrigo, M.A., Panizza, M., 2014. Electrochemical advanced oxidation processes: Today and tomorrow. A review. Environ. Sci. Pollut. Res. 21, 8336–8367. https://doi.org/10.1007/s11356-014-2783-1

Steter, J.R., Brillas, E., Sirés, I., 2018. Solar photoelectro-Fenton treatment of a mixture of parabens spiked into secondary treated wastewater effluent at low input current. Appl. Catal. B: Environ. 224, 410–418. http://dx.doi.org/10.1016/j.apcatb.2017.10.060

Teodosiu, C., Gilca, A.F., Barjoveanu, G., Fiore, S., 2018. Emerging pollutants removal through advanced drinking water treatment: A review on processes and environmental performances assessment. J. Clean. Prod. 197, 1210–1221. https://doi.org/10.1016/j.jclepro.2018.06.247

Thiam, A., Sirés, I., Salazar, R., Brillas, E., 2018. On the performance of electrocatalytic anodes for photoelectro-Fenton treatment of synthetic solutions and real water spiked with the herbicide chloramben. J. Environ. Manage. 224, 340–349. https://doi.org/10.1016/j.jenvman.2018.07.065

Thiam, A., Salazar, R., 2019. Fenton-based electrochemical degradation of metolachlor in aqueous solution by means of BDD and Pt electrodes: influencing factors and reaction pathways.

582 Environ. Sci. Pollut. Res. 26, 2580–2591. https://doi.org/10.1007/s11356-018-3768-2
583 Vasudevan, S., Oturan, M.A., 2014. Electrochemistry: As cause and cure in water pollution-An
584 overview. Environ. Chem. Lett. 12, 97–108. https://doi.org/10.1007/s10311-013-0434-2
585 Wang, B., Ni, B.-J., Yuan, Z., Guo, J., 2019. Cometabolic biodegradation of cephalexin by enriched
586 nitrifying sludge: Process characteristics, gene expression and product biotoxicity. Sci. Total
587 Environ. 672, 275–282. https://doi.org/10.1016/j.scitotenv.2019.03.473
588 Xu, J., Li, Y., Qian, M., Pan, J., Ding, J., Guan, B., 2019. Amino-functionalized synthesis of MnO_2-
589 NH_2-GO for catalytic ozonation of cephalexin. Appl. Catal. B: Environ. 256, 117797.
590 https://doi.org/10.1016/j.apcatb.2019.117797
591 Ye, Z., Guelfi, D.R.V., Álvarez, G., Alcaide, F., Brillas, E., Sirés, I., 2019. Enhanced electrocatalytic
592 production of H_2O_2 at Co-based air-diffusion cathodes for the photoelectro-Fenton treatment of
593 bronopol. Appl. Catal. B: Environ. 247, 191–199. https://doi.org/10.1016/j.apcatb.2019.01.029
594 Ye, Z., Padilla, J.A., Xuriguera, E., Brillas, E., Sirés, I., 2020a. Magnetic MIL(Fe)-type MOF-derived
595 N-doped nano-ZVI@C rods as heterogeneous catalyst for the electro-Fenton degradation of
596 gemfibrozil in a complex aqueous matrix. Appl. Catal. B: Environ. 266, 118604.
597 https://doi.org/10.1016/j.apcatb.2020.118604
598 Ye, Z., Padilla, J.A., Xuriguera, E., Beltran, J.L., Brillas, E., Sirés, I., 2020b. A highly stable metal–
599 organic framework-engineered FeS_2/C nanocatalyst for heterogeneous electro-Fenton treatment:
600 Validation in wastewater at mild pH. Environ. Sci. Technol. (in press).
601 https://doi.org/10.1021/acs.est.9b07604
602 Zhang, M.H., Dong, H., Zhao, L., Wang, D.X., Meng, D., 2019a. A review on Fenton process for
603 organic wastewater treatment based on optimization perspective. Sci. Total Environ. 670, 110–
604 121. https://doi.org/10.1016/j.scitotenv.2019.03.180
605 Zhang, Y., Wang, A., Ren, S., Wen, Z., Tian, X., Li, D., Li, J., 2019b. Effect of surface properties of
606 activated carbon fiber cathode on mineralization of antibiotic cefalexin by electro-Fenton and

photoelectro-Fenton treatments: Mineralization, kinetics and oxidation products. Chemosphere 221, 423–432. https://doi.org/10.1016/j.chemosphere.2019.01.016

Zhou, S., Gan, M., Zhu, J., Li, Q., Jie, S., Yang, B., Liu, X., 2015. Catalytic effect of light illumination on bioleaching of chalcopyrite. Bioresour. Technol. 182, 345–352. https://doi.org/10.1016/j.biortech.2015.02.010

Zhou, M., Oturan, M.A., Sirés, I., 2018. Electro-Fenton Process: New Trends and Scale-Up, Springer Nature, Singapore.

Figure captions:

Fig. 1. XRD pattern of clean chalcopyrite before use.

Fig. 2. XPS spectrum of clean chalcopyrite before use, showing (a) Fe 2*p* and (b) Cu 2*p*.

Fig. 3. (a) TEM micrograph of clean chalcopyrite before use, (b) EDS mapping showing the Fe distribution, (c) EDS mapping of Cu and (d) EDS analysis.

Fig. 4. Released Fe^{2+} concentration vs. initial chalcopyrite content after 30 min of stirring of milled mineral powder in 100 mL of Milli-Q water exposed to compressed air bubbling at 0.6 L min^{-1}.

Fig. 5. (a) Variation of cephalexin concentration with electrolysis time for the treatment of 100 mL of a 50 mg L^{-1} drug solution with 0.050 M Na_2SO_4 and 1 g L^{-1} chalcopyrite at 25 ºC, using a stirred IrO_2/air-diffusion cell at 50 mA cm^{-2}. Method: (●) HEF (○) HPEF. The kinetic analysis considering a pseudo-first-order reaction is presented in the inset panel. (b) Comparison of percentages of cephalexin removal after 15 min of different treatments.

Fig. 6. Effect of chalcopyrite content on the change of cephalexin concentration with electrolysis time for the HPEF treatment of 100 mL of 50 mg L^{-1} antibiotic solutions with 0.050 M Na_2SO_4 at 25 ºC, using a stirred IrO_2/air-diffusion cell at 50 mA cm^{-2}. [Chalcopyrite]: (▲) 0.5 g L^{-1}, (○) 1 g L^{-1}, (■) 2 g L^{-1} and (◇) 3 g L^{-1}. The pseudo-first-order kinetic analysis is depicted in the inset panel.

Fig. 7. Time course of (a) cephalexin concentration, (b) TOC removal and (c) mineralization current efficiency for the treatment of 100 mL of 50 mg L^{-1} antibiotic solutions with 0.050 M Na_2SO_4 at 25 ºC, using a stirred IrO_2/air-diffusion cell at 50 mA cm^{-2}. Method: (□) HEF with 1 g L^{-1} chalcopyrite, (○) HPEF with 1 g L^{-1} chalcopyrite, (◆) EF with 0.05 mM Fe^{2+} + 0.05 mM Cu^{2+} and (◇) PEF with 0.05 mM Fe^{2+} + 0.05 mM Cu^{2+}. The inset panel shows the kinetic analysis considering a pseudo-first-order reaction.

Fig. 8. Percentage of cephalexin removal vs electrolysis time for successive HPEF treatments of 100 mL of suspensions containing 50 mg L^{-1} antibiotic, 0.050 M Na_2SO_4 and 1 g L^{-1} chalcopyrite at 25 ºC, using a stirred IrO_2/air-diffusion cell at 50 mA cm^{-2}.

Fig. 9. Evolution of carboxylic acid concentrations with electrolysis time for the treatment of 50 mg L^{-1} antibiotic solutions under the same conditions described in Fig. 5. (●) Oxalic acid by HEF, (○) oxalic acid by HPEF (■) oxamic acid by HEF and (□) oxamic acid by HPEF.

Fig. 10. Proposed reaction pathway for the degradation of cephalexin by HEF or HPEF.

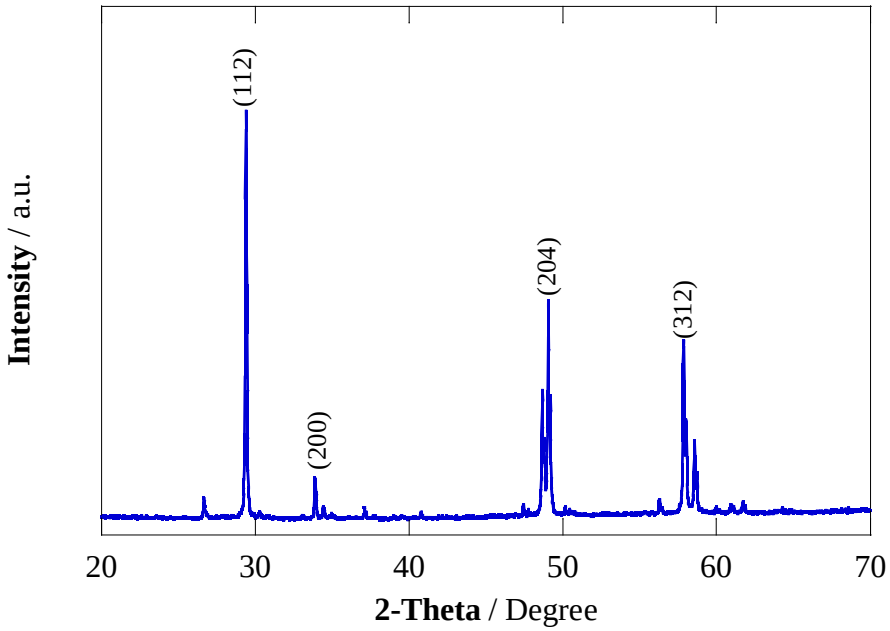
(112)
(200)
(204)
(312)
Intensity / a.u.
20
30
40
50
60
70
2-Theta / Degree

Fig. 1

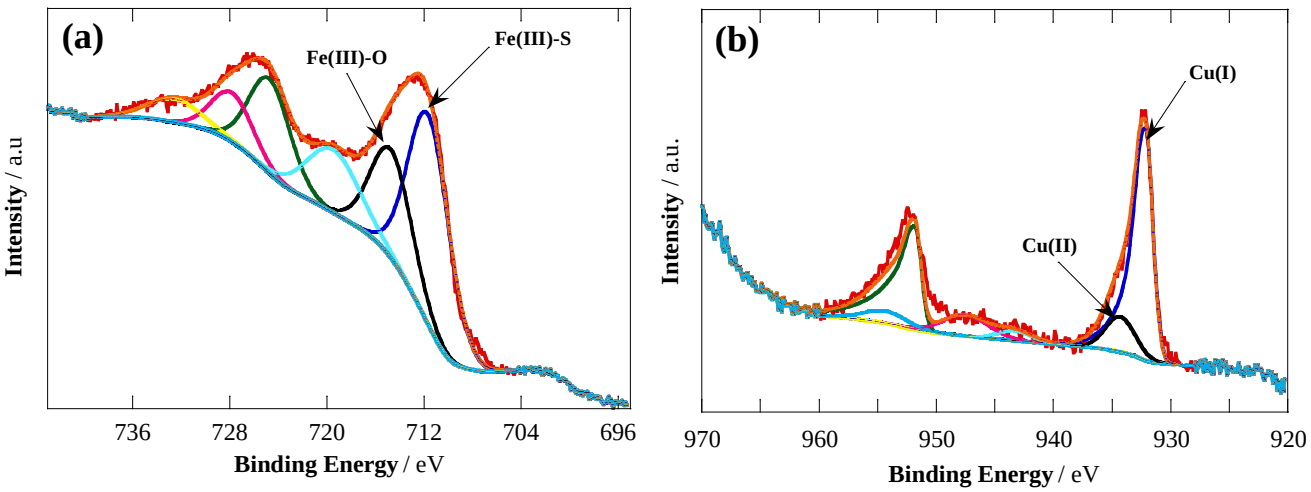
(a)
Fe(III)-O
Fe(III)-S
Intensity / a.u
736
728
720
712
704
696
Binding Energy / eV
(b)
Cu(I)
Cu(II)
Intensity / a.u.
970
960
950
940
930
920
Binding Energy / eV

Fig. 2

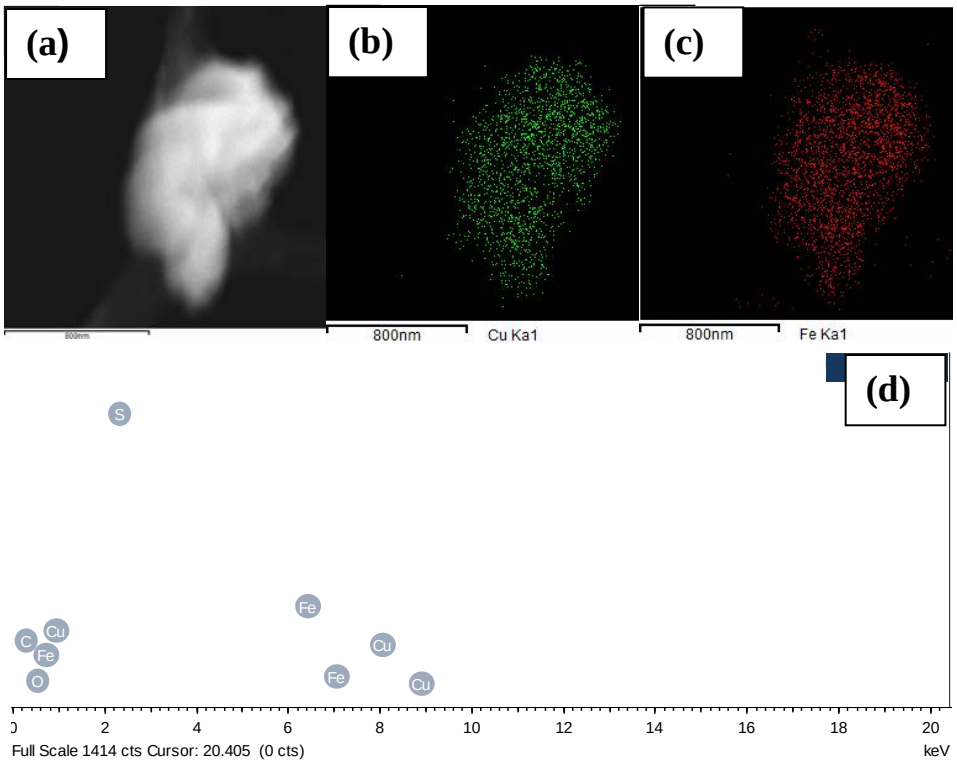
(a)
(b)
(c)
(d)
800nm
Cu Ka1
800nm
Fe Ka1
S
Fe
C
Cu
Fe
Cu
O
Fe
Cu
0
2
4
6
8
10
12
14
16
18
20
Full Scale 1414 cts Cursor: 20.405 (0 cts)
keV

Fig. 3

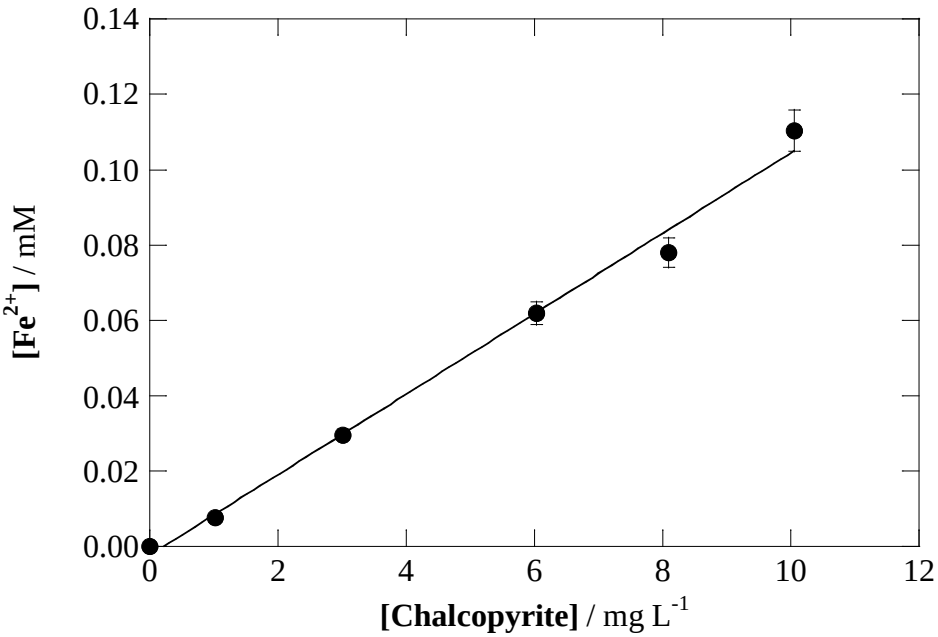
0.14
0.12
0.10
0.08
0.06
0.04
0.02
0.00
0
2
4
6
8
10
12
[Fe2+] / mM
[Chalcopyrite] / mg L-1

Fig. 4

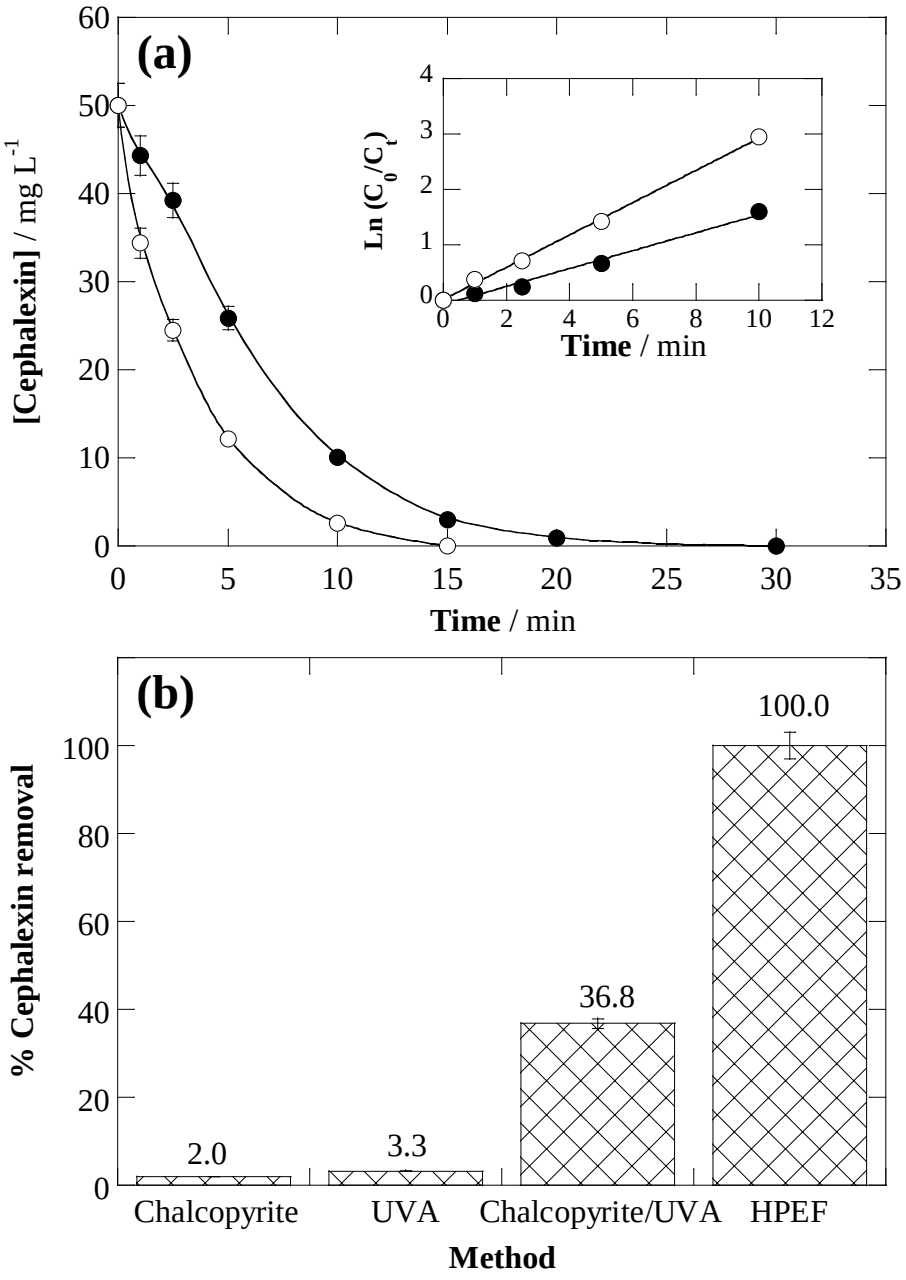
(a)
[Cephalexin] / mg L-1
Time / min
Ln (C0/Ct)
Time / min
(b)
% Cephalexin removal
2.0
3.3
36.8
100.0
Chalcopyrite
UVA
Chalcopyrite/UVA
HPEF
Method

Fig. 5

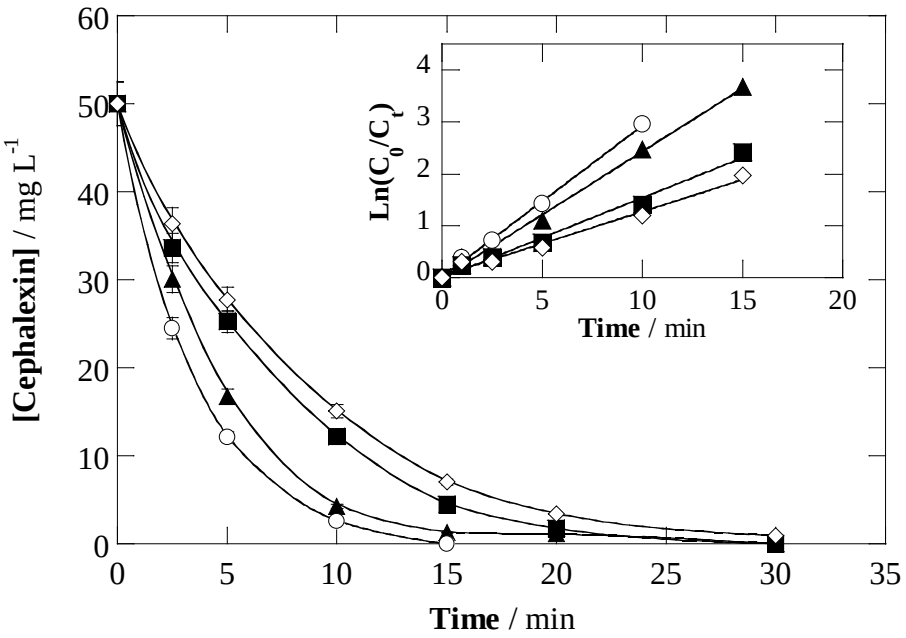

Fig. 6

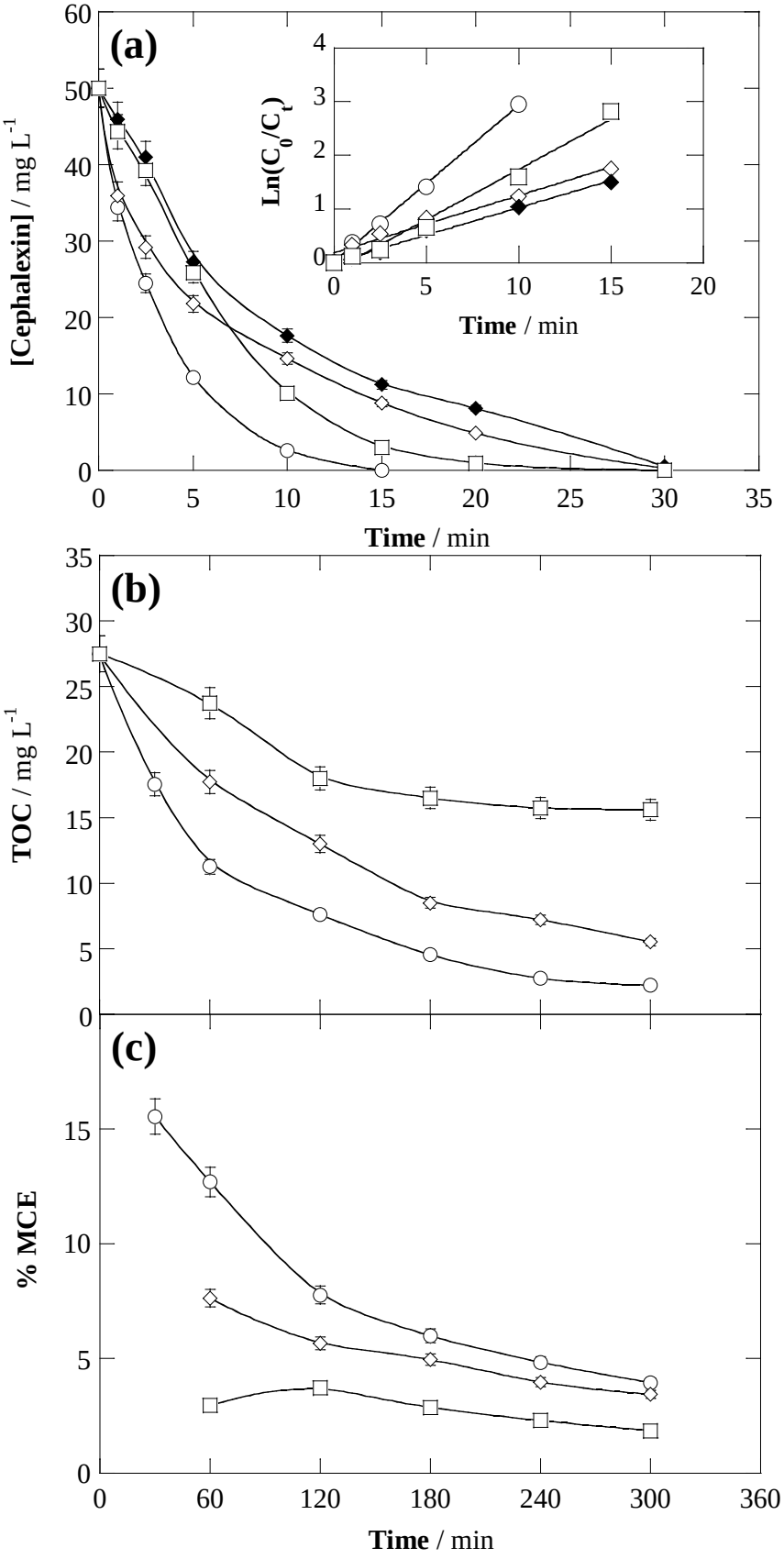
(a)
[Cephalexin] / mg L-1
Time / min
Ln(C0/Ct)
Time / min
(b)
TOC / mg L-1
(c)
% MCE
Time / min

Fig. 7

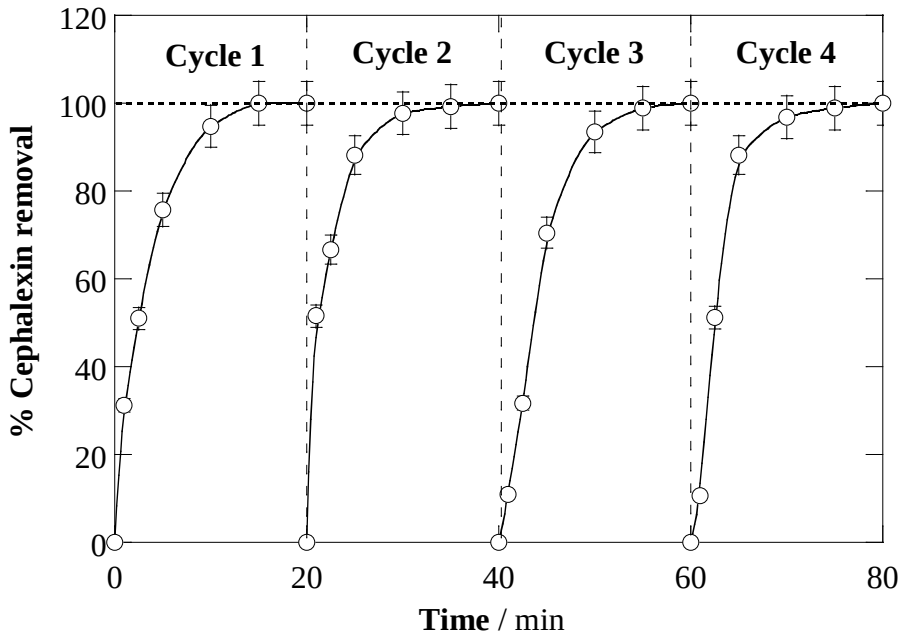
Cycle 1
Cycle 2
Cycle 3
Cycle 4
% Cephalexin removal
Time / min
0
20
40
60
80
100
120

Fig. 8

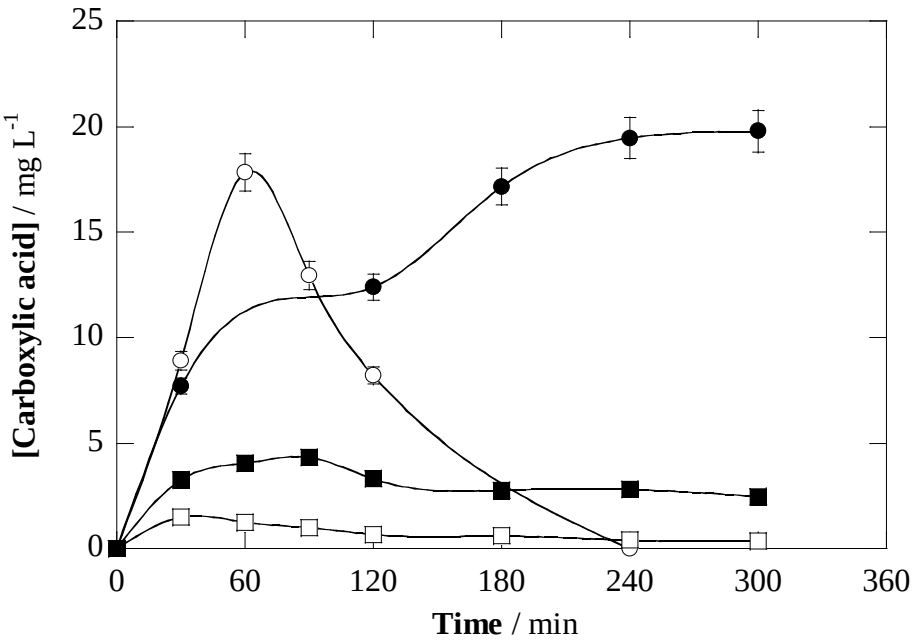
25
20
15
10
5
0
0
60
120
180
240
300
360
[Carboxylic acid] / mg L-1
Time / min

Fig. 9

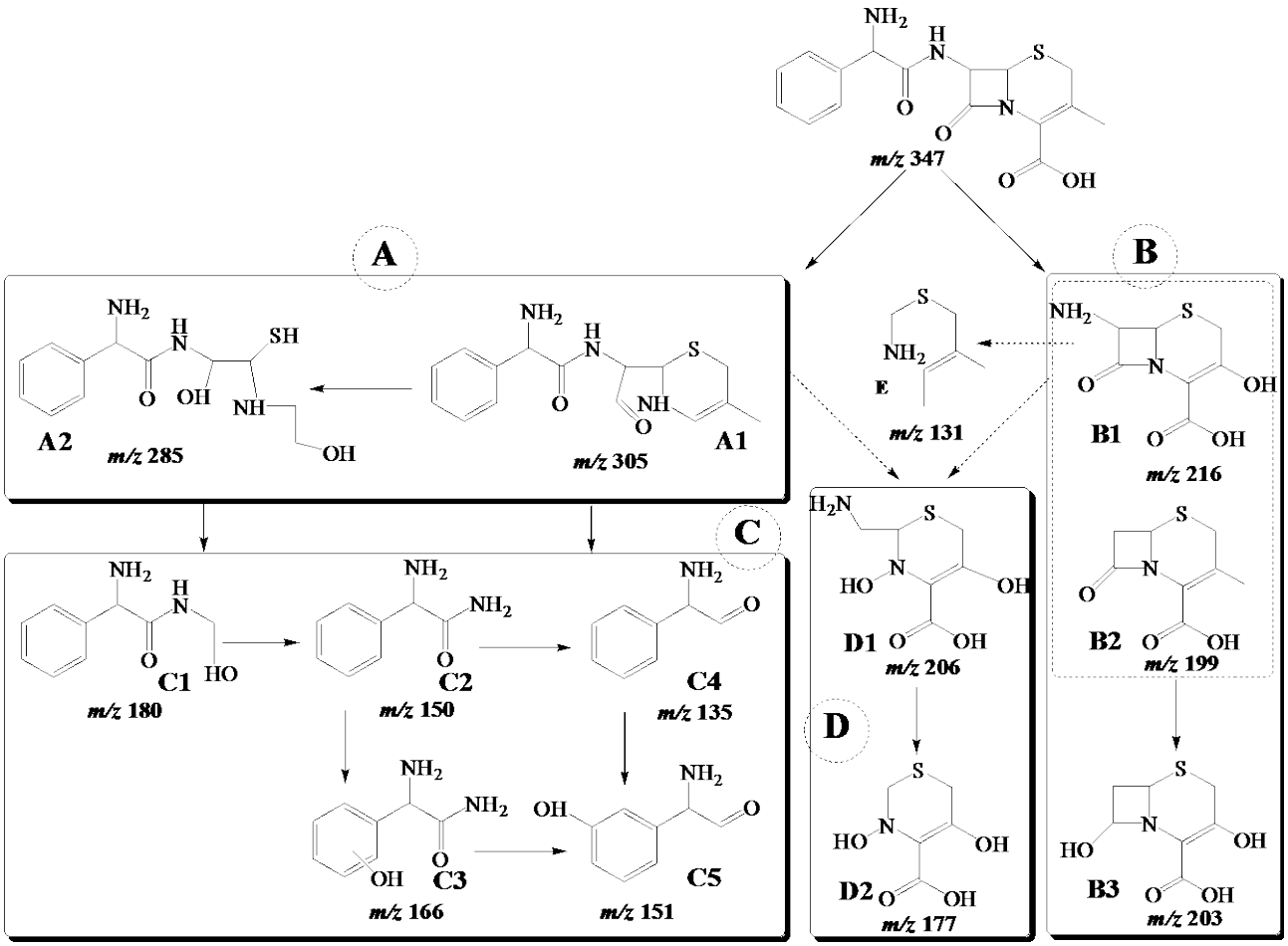
m/z 347
A
B
A2
m/z 285
A1
m/z 305
E
m/z 131
B1
m/z 216
B2
m/z 199
B3
m/z 203
C
C1
m/z 180
C2
m/z 150
C4
m/z 135
C3
m/z 166
C5
m/z 151
D
D1
m/z 206
D2
m/z 177

Fig. 10

811 **Table 1.** Chemical composition of the chalcopyrite powder before use.

Element	As	Cu	Fe	Mo	Pb	S	Zn
Content (wt.%)	0.32	24.10	26.40	0.79	0.07	32.95	0.41

812

813

Table 2. Pseudo-first-order rate constant with the squared regression coefficient, and percentage of cephalexin removal obtained at 15 min, for the treatment of 50 mg L^{-1} cephalexin with 0.050 M Na_2SO by several Fenton-based EAOPs.

Method	**[Chalcopyrite](g L^{-1})**	***I* (mA)**	**k_1 (10^{-3} s^{-1})**	**R^2**	**% Cephalexin removal**
HEF	1.0	125	3.12	0.985	94.0
HPEF	0.5	125	4.05	0.995	97.4
	1.0	125	4.85	0.998	100
	2.0	125	2.57	0.989	91.1
	3.0	125	2.05	0.984	85.9
	1.0	250	7.04	0.993	99.1
	1.0	62.5	2.16	0.979	87.7
	[Catalyst] (mM)				
EF	0.05 Fe^{2+} + 0.05 Cu^{2+}	125	1.69	0.996	77.8
PEF	0.05 Fe^{2+}+ 0.05 Cu^{2+}	125	1.77	0.985	82.4